JOURNAL OF CATALYSIS **179,** 400–412 (1998)
ARTICLE NO. CA982244

Catalytic Combustion of Volatile Organic Compounds over La-Based Perovskites

S. Irusta,[1] M. P. Pina, M. Menéndez, and J. Santamaría[2]

Department of Chemical and Environmental Engineering, University of Zaragoza, 50.009 Zaragoza, Spain

Received January 23, 1998; revised July 31, 1998; accepted July 31, 1998

$LaCoO_3$, $LaMnO_3$, $La_{0.8}Sr_{0.2}CoO_3$, and $La_{0.8}Sr_{0.2}MnO_3$ perovskites have been used for the combustion of VOCs (toluene and methyl-ethyl-ketone) in air, at temperatures between 200 and 300°C. Reaction tests have been carried out using the single compounds, as well as binary mixtures in different proportions. Several characterization techniques have been employed in order to gain insight into the changes taking place on the catalyst surface, especially during the combustion of binary mixtures. The discussion attempts to relate these changes to the catalytic performance observed.

INTRODUCTION

Perovskite-type oxides have consistently been proposed during the last two decades as alternative catalysts for deep oxidation of hydrocarbons. Typical catalysts are supported Pt or Pd and single or mixed metal oxides. The use of perovskites has been advocated especially in applications involving high temperatures and oxygen and steam-rich atmospheres, where their substantial thermal stability comes into play. This was recognized since the early 1970s, when perovskites were proposed as promising automobile exhaust catalysts (1), with a lower cost compared to their noble metal counterparts. The perovskites can be represented by the general formula $A_1A_2B_1B_2O_3$, where A_1 is chosen among lanthanides (generally La, but sometimes Ce, Pr, or Nd), and A_2 among alkaline earth metals (Ca, Sr, Ba); the B_1 and B_2 positions are occupied by transition metals (Co, Mn, Fe, Cr, Cu, V), or noble metals. A_2 and B_2 correspond to the substitution of part of the A_1 and B_1 ions, respectively. In particular, the replacement of part of the La^{3+} ion by Sr^{2+} has often resulted in a considerable increase in the combustion activity (2).

Under suitable circumstances, the activity of perovskites can be very considerable, even comparable to that of noble-metal catalysts, as demonstrated for instance by Arai *et al.* (3). These authors found similar light-off (50% conversion) temperatures for $LaCoO_3$, $La_{0.8}Sr_{0.2}CoO_3$, $La_{0.8}Sr_{0.2}MnO_3$, and Pt (1 wt%)/Al_2O_3 in the combustion of methane under comparable conditions, despite a much lower surface area (3–5 m^2/g) on the part of the perovskites. In fact, to obtain the perovskite structure while preserving a sufficiently high surface area constitutes the main challenge in the development of these catalysts. The preparation of perovskite oxides involves a solid state reaction of the precursor oxides to form the characteristic ABO_3 structure. This requires significant exposure times at high temperatures, leading to a low specific surface of the catalyst.

In order to circumvent this limitation, a number of alternative preparation methods has been tried, with the aim of reducing the firing temperature necessary for perovskite synthesis. These methods include the so-called ethylene glycolate, carbonyl, and citrate methods (4), as well as other precursor salts, such as oxalate, acetate, or nitrate salts. The citrate precursor method seems to be very effective to increase the surface area of the synthesized perovskites and has been used with some frequency in recent years (5). The preservation of surface area is critical, since it has often been observed that the reaction rate over bulk perovskites is directly proportional to the BET surface area (6). It should be noted, however, that the higher surface areas so obtained (a few tens of square meters per gram of catalyst) are often reduced considerably by sintering at the reaction conditions. This has prompted some interesting efforts to support perovskites onto thermally stable oxides such as stabilized alumina, aluminates with a spinel structure or cordierite. The main problem with this approach is the affinity of the B cation in the perovskite towards the support. This can partially be overcome by the use of cations such as Cr^{3+} which are less apt to react with the alumina support (7).

Most of the development work carried out with perovskites to date has been oriented towards relatively high-temperature applications, such as methane combustion (3, 4, 7, 8). However, with perovskites synthesized by the citrate method and similar ones, where high reaction temperatures mean a rapid loss of surface area by sintering, the application to reactions that run at lower temperatures

[1] On leave from INCAPE, Argentina.
[2] Corresponding author. E-mail: iqcatal@posta.unizar.es. Phone: +34 976 761153. Fax: +34 976 761159.

0021-9517/98 $25.00

is of interest. The catalytic combustion of VOCs (volatile organic compounds) is a typical reaction where low temperatures are sought in order to save on energy costs (since VOCs are usually present in diluted streams), and also to avoid the formation of nitrogen oxides. A few works in the literature have previously addressed the use of perovskites for this process; among them, Chang and Weng (9) carried out the deep oxidation of toluene over $La_{0.8}Sr_{0.2}CoO_3$, and Lintz and Wittstock (10) studied the combustion of several VOCs on $LaMnO_3$.

In this work, the use of perovskites ($A_1 = La$, $A_2 = Sr$, $B_1 = Co$ or Mn) for the combustion of toluene and methyl-ethyl-ketone, as VOCs contained in an air stream, has been investigated. A battery of characterization techniques has been used, in order to gain insight into the changes taking place on the catalyst surface and to relate these changes to the catalytic performance observed. Special attention has been paid to the behavior of the perovskite catalysts regarding the combustion of binary mixtures. Mixture effects have been shown to be rather complex, even in systems such as supported noble metal catalysts (e.g., (11, 12)) which are considerably simpler than those studied in this work.

EXPERIMENTAL

Catalyst Preparation

The perovskites prepared using the so-called citrate method were $LaMnO_3$, $LaCoO_3$, $La_{0.8}Sr_{0.2}MnO_{3-x}$, and $La_{0.8}Sr_{0.2}CoO_{3-x}$. For simplicity, these will be denoted as La-Mn, La-Co, La-Sr-Mn, and La-Sr-Co in the remainder of this work. The salts used were initially nitrates, each of which (La, Mn, Co, Sr), was dissolved in deionized water. After titration, the solutions were mixed in the desired proportions and N moles of citric acid were added (N being equal to the total number of moles of La and Sr, Co, or Mn). The solution was maintained at 100°C for 12 h, which rendered a porous gel. This was then ground to the appropriate particle size, and calcined in two stages, first at 300°C for 30 min, and then at a higher temperature (usually 600°C, but sometimes 800 or 1000°C), for 2 h. In both cases the sample was heated to the desired calcination temperature at a rate of 2°C/min.

Catalyst Characterization

The phases present in the catalysts prepared were characterized by X-ray diffraction analysis (XRD), in a Rigaku/Max system difractometer using Ni-filtered CuKα radiation, at a scan rate of 0.02° per second, between 5–80°. The BET surface area was determined by N_2 adsorption–desorption measurements in Pulse-Chemisorb 2700 equipment.

Temperature-programmed reduction (TPR) experiments were carried out on freshly calcined samples, and on samples pretreated with VOC-containing air and N_2 streams. The TPR experiments were performed in a quartz reactor loaded with 100 mg of catalyst, under a mass flow-controlled stream containing 5% H_2 in N_2, with a heating rate of 5°C/min, from room temperature to 900°C.

Diffuse reflectance (DRIFT) data were obtained using a Mattson Research Series spectrometer, equipped with a Spectra-Tech high pressure/temperature environmental chamber and a nitrogen-cooled MCT detector. Approximately 30 mg of a powdered perovskite sample were loaded into the DRIFT cell, to which the VOC-containing gas stream was fed using a system analogous to that described below for the reaction experiments. DRIFT spectra of the catalyst samples under different atmospheres (inert, air, reaction) and temperatures were recorded by co-adding a fixed number of scans (300 in steady-state experiments, 140 in transient experiments) at a resolution of 4 cm^{-1}. Positions, number of bands, and intensities were established from the second-derivative spectra. In order to avoid any interference from material remaining on the surface, a new catalyst sample was used in every DRIFT experiment. When transient DRIFT experiments were carried out, a step change in the feed to the spectrometer was generated, and the evolution with time of the characteristic IR bands was followed.

Reaction Experiments

The reaction system employed has been described previously (13). It consisted of: (i) A feed section in which a mass flow controlled stream (air) was saturated with the selected organic compound and mixed with a second mass flow controlled air stream to give the desired VOC partial pressure (from 10 to 515 Pa). Saturation was achieved by bubbling the air stream through a series of three flasks containing the VOC, the first at room temperature and the other two immersed in an ice bath (at 0°C). A sintered glass frit was used to disperse the air in very small bubbles throughout the liquid VOC. Both toluene and methyl-ethyl-ketone (MEK) were used in the reactor feed, as representative of aromatic and oxygenated VOCs, respectively. The volatile organic compounds could be fed to the reactor alone or in a binary mixture, in which case the saturation train was duplicated, and the reactor feed stream consisted of two VOC-saturated air streams mixed with a third air stream for dilution. (ii) A quartz, 8-mm ID reactor, loaded with 50 mg of ground perovskite (100–250 μm particle size) and operated at atmospheric pressure. In order to facilitate temperature control, the perovskite samples were diluted in quartz in a 1 : 5 ratio. The temperature of the reactor was measured by a thermocouple directly embedded in the catalyst bed, and kept at the desired value by means of an external electrical furnace. (iii) An analysis section, comprising an on-line gas chromatograph (FID detector) and CO and CO_2 analyzers, which were used to check mass balances. A set of

valves allowed bypassing the reactor to lead the feed stream directly into the gas chromatograph sampling loop, which provided a direct measurement of the VOC concentrations fed. WHSV values were calculated as the ratio between the total mass flow of the reactant stream (air + VOCs) and the mass of catalyst used.

In a few cases, transient reaction experiments were run, in order to correlate the changes observed in the catalyst surface by transient DRIFT analysis with the variation of the catalytic activity. In order to obtain a fast response, an on-line quadrupole mass spectrometer (HIDEN HAL 2/201) was used to continuously monitor the reactor exit stream. The transient reaction experiments were conducted by first oxidizing the catalyst sample in air at the reaction temperature and then shifting the air feed to a VOC-saturated air stream, using a 4-way valve.

RESULTS AND DISCUSSION

Catalyst Characterization

The composition, calcination temperatures, BET areas, and average particle size and crystalline phases identified from XRD for the different perovskites studied in this work are given in Table 1. It can be seen that, for a given type of perovskite, the measured surface area strongly depends on the calcination temperature (unless otherwise indicated in all cases the calcination time was 2 h). Thus, for $LaCoO_3$, an increase of calcination temperature from 600 to 800°C leads to the loss of about 67% of the surface area, and when the calcination temperature used was 1000°C then the loss of surface area with respect to the 600°C sample reached 95%. The loss of surface area for increasing temperatures correlates well with the increase in the average crystal size determined from XRD, as shown in Table 1. On the other hand, the results of XRD analysis show that there was perovskite formation in all the samples prepared by the citrate method in which calcination temperatures of at least 600°C were used (Fig. 1), although the amount of impurities and the degree of crystallinity varied considerably for the different perovskites and also for the same perovskite when calcined at different temperatures (Table 1). The introduction of Sr in the La-Co perovskites results in a smaller crystal size (and a higher BET area), along with a noticeable decrease in the degree of crystallinity for a given calcination temperature. In addition, part of the Sr in the La-Sr-Co perovskite was present as $SrCO_3$ outside the perovskite structure. In the La-Mn perovskites calcined at 600°C (with and without addition of Sr), tetragonal La_2CO_5 (and possibly hexagonal La_2O_3) species were present, which became incorporated into the perovskite structure with an additional calcination of 2 h at 800°C. In general, it can be said that the addition of Sr to the precursor solutions of La-Co and La-Mn perovskites gives rise to a less crystalline perovskite, with a smaller crystal size and a higher surface area. The possible presence of the individual metal compounds was specifically investigated in the XRD patterns of the different perovskites, but these were not detected,

TABLE 1

Physico-Chemical Characterization of the Solids Prepared

Sample/catalyst	Calcination temperature (°C)	L (A)[a]	XRD structure	BET area m^2/g
1/La-Mn	600	2.09	$LaMnO_{3.07}$ perosvkite with orthorhombic structure. Presence of amorphous phase and La_2CO_5 impurities.	14.9
2/La-Mn	600[b]	2.29	$LaMnO_{2.875}$ perosvkite with orthorhombic structure. Presence of amorphous phase and La_2CO_5 impurities.	14.6
3/La-Mn	800	3.02	Pure perovskite structure, well crystallized. Stochiometry between $LaMnO_{3.07}$ and $LaMnO_{3.15}$.	12.9
4/La-Sr-Mn	600	1.78	Monoclinic perovskite structure. Presence of amorphous phase and La_2CO_5 impurities.	32.1
5/La-Sr-Mn	800	4.20	Monoclinic perovskite structure well crystallized.	18.7
6/La-Co	600	3.16	Rhombohedral perovskite structure.	12.1
7/La-Co	800	5.05	Rhombohedral perovskite structure. Higher crystallinity than sample 6.	3.9
8/La-Co	1000	5.60	Rhombohedral perovskite structure. Higher crystallinity than samples 6 and 7.	0.5
9/La-Sr-Co	600	2.21	Perovskite $La_{0.8}Sr_{0.2}CoO_{3-x}$($x < 0.1$) with rhombohedral structure. Presence of La_2CO_5 and $SrCO_3$ impurities.	13.0
10/La-Sr-Co	800	3.88	Perovskite $La_{0.8}Sr_{0.2}CoO_{3-x}$($x < 0.1$) with orthorhombic and rhombohedral structure. Higher crystallinity than sample 9. Less $SrCO_3$ impurities.	10.0

[a] Characteristic length calculated from the main XRD band.
[b] Reduced at 600°C.

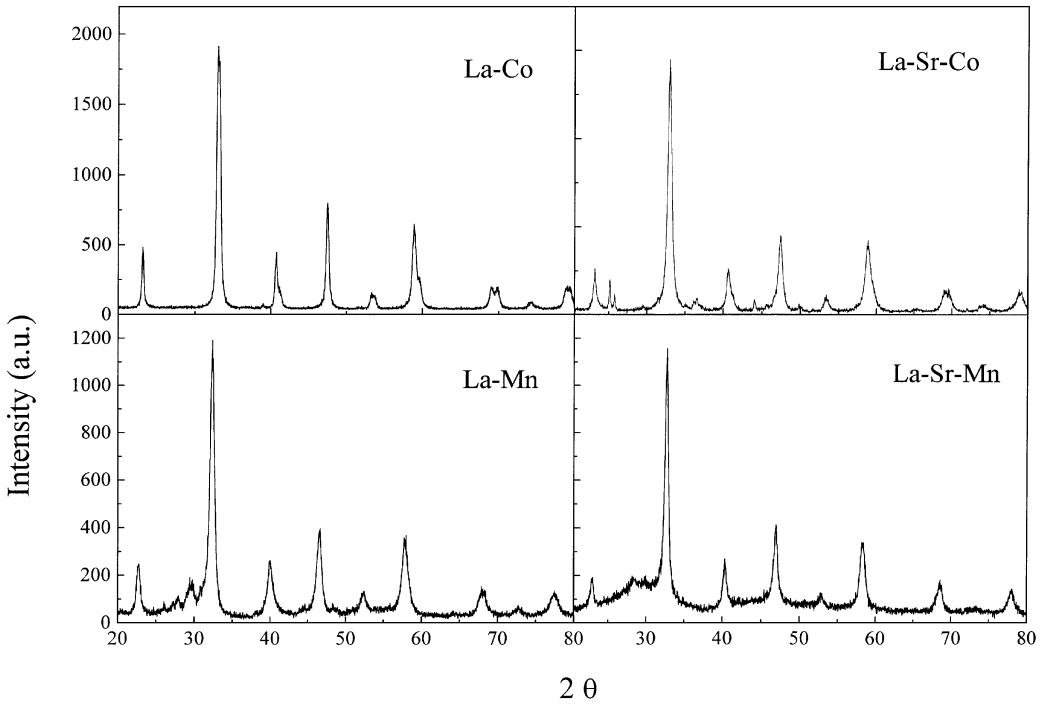

FIG. 1. XRD patterns of the different perovskites studied in this work, obtained with a calcination temperature of 600°C.

except for the case of La_2CO_5 and La_2O_3 in the cases already mentioned.

TPR Experiments

The TPR diagram of the $LaCoO_3$ perovskite is given in Fig. 2A. There are three main reduction bands at 242°C, 395°C (with a second peak at 370°C), and 555°C. The H_2 consumption observed below 300°C is likely related to the reduction of perovskite microcrystals, whose presence in the synthesized solids is indicated by the higher baseline level in the XRD patterns. According to the experimental work of Wachowski *et al.* (14), who reduced $LaCoO_3$ under 10% H_2 in N_2, the low temperature TPR peaks would be associated to the reduction of $LaCoO_3$ to an intermediate oxygen-deficient compound, according to

$$LaCoO_3 \Rightarrow LaCo_xO_{3-y} + (1 - x)Co + y/2O_2.$$

The second reduction process, leading to La_2O_3 and Co^o takes place above 550°C. The position of the peaks representing both reduction processes depends on the calcination temperature used. Thus, in separate TPR experiments the position of the peaks consistently shifted towards higher temperatures as the calcination temperature was increased. As can be seen in Fig. 2A for $LaCoO_3$, the 555°C peak shifted to 590°C for perovskites calcined at 800°C, and to 642°C when the calcination temperature used was 1000°C. This is in agreement with the sintering process just described, which along with the decrease of surface area produces a narrower crystal size distribution, with a higher mean crystal size. The increased diffusional resistance gives rise to a displacement towards higher temperatures of the reduction peaks in TPR experiments.

The replacement of part of the La by Sr to give $La_{0.8}Sr_{0.2}CoO_{3-x}$ (i.e., La-Sr-Co perovskite in Figs. 1 and 2B) gives a less crystalline structure which is easier to reduce, as seen in Fig. 2B, where the reduction of perovskite microcrystals now starts below 200°C. Another important difference with the TPR diagram for the La-Co perovskite is the presence of a new peak at 750°C, attributed to the decomposition of the $SrCO_3$ species detected by XRD. This attribution is supported by a separate experiment (not shown) in which Sr citrate was calcined at 600°C, giving crystals which were positively identified as $SrCO_3$ by XRD, and a single TPR peak at around 850°C. The lower temperature of the TPR peak for $SrCO_3$ in Fig. 2A is consistent with a considerably smaller crystal size.

Figure 3 shows the corresponding TPR diagrams for La-Mn and La-Sr-Mn perovskites. In the La-Mn perovskite prepared at 600°C, two main peaks appear, at 438 and 750°C. In order to confirm the existence of perovskite species with an intermediate degree of reduction, an experiment was carried out in which the original La-Mn perovskite was reduced up to 600°C, following the same operating protocol as in the TPR experiments, and then subjected to XRD analysis. The results (see Table 1) showed the existence of an oxygen-deficient perovskite, with a composition $LaMnO_{2.875}$. Therefore, the low temperature peak in the

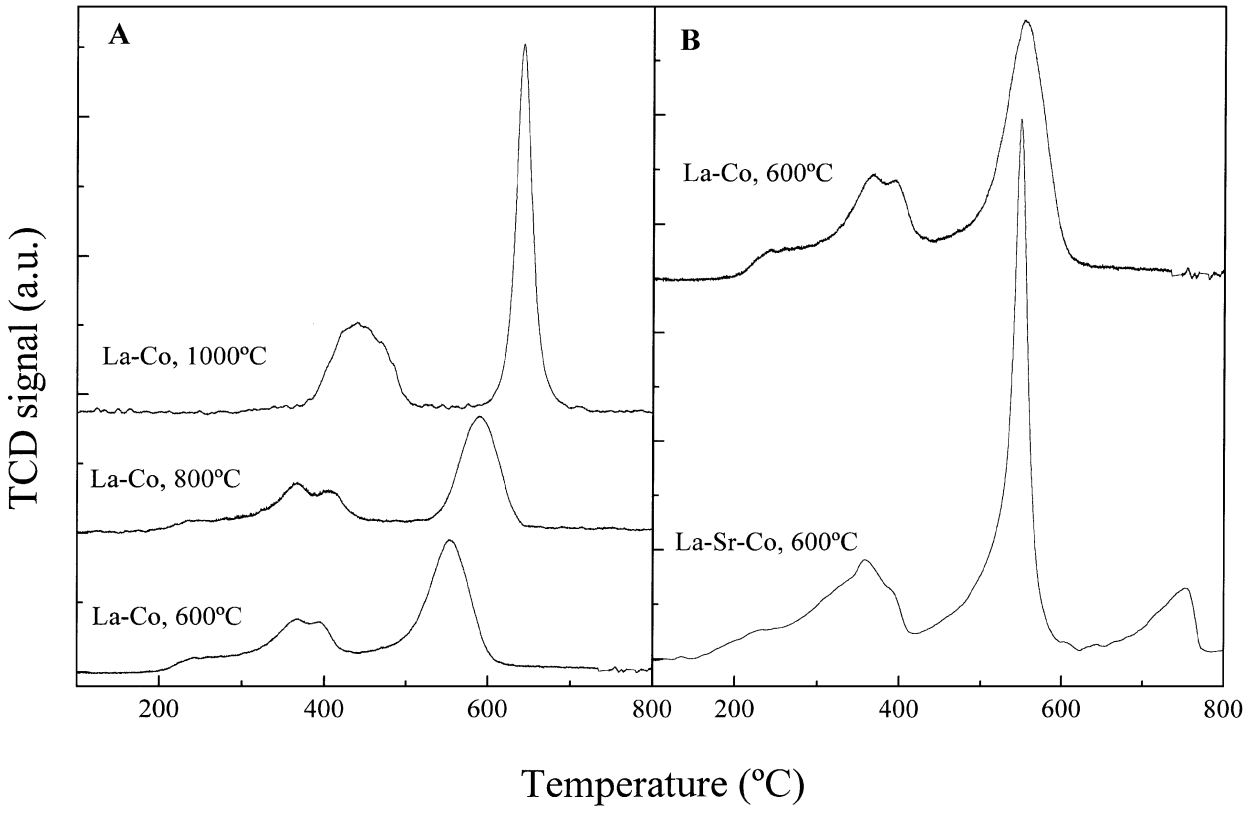

FIG. 2. Results of the temperature programmed reduction (TPR) experiments for the La-Co and La-Sr-Co perovskites, obtained with calcination at different temperatures.

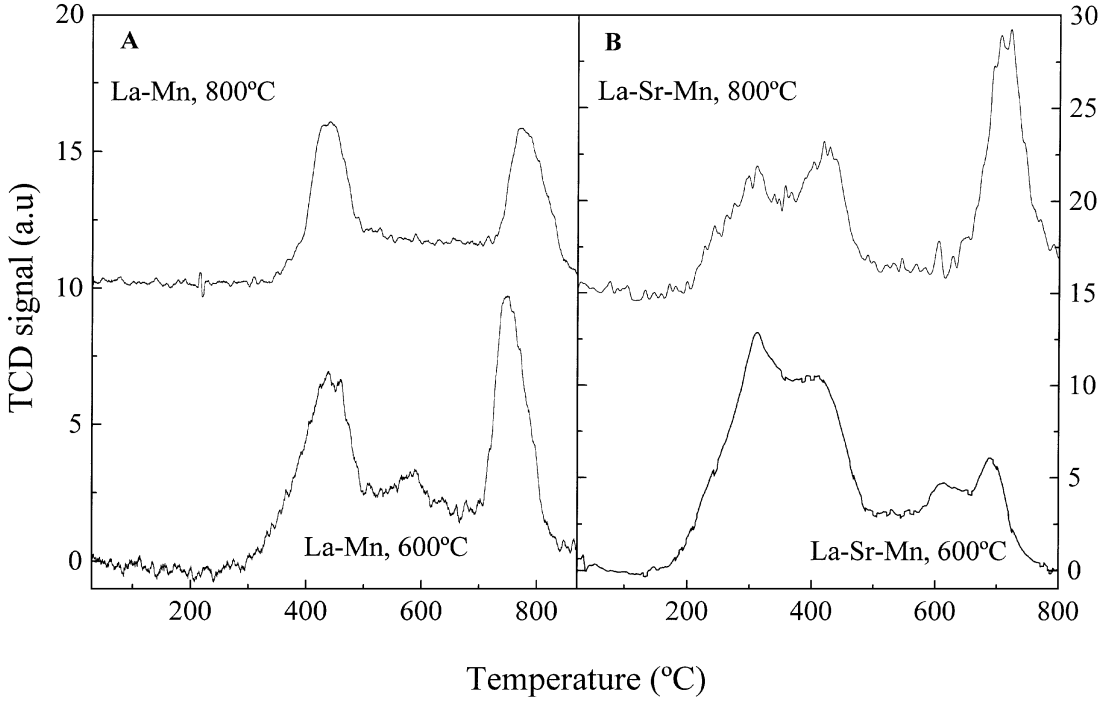

FIG. 3. Results of the temperature programmed reduction (TPR) experiments for the La-Mn and La-Sr-Mn perovskites, obtained with calcination at different temperatures. NOTE: The *y*-axis scale is different in Figs. 3a and 3b.

TPR diagram can be attributed to the reduction of the original perovskite to the intermediate $LaMnO_{2.875}$ species (a similar behavior to that discussed for the La-Co perovskite), while the high-temperature peak would correspond to the reduction of the intermediate species to the individual oxides. When a further calcination of 2 h in air at 800°C was carried out, the XRD patterns (Table 1) showed a perovskite with a rhombohedrally distorted structure, with composition $LaMnO_{3.15}$. The TPR diagram in Fig. 3A shows that for the sample calcined at 600°C, the low-temperature (below 500°C) reduction accounted for 27% of the total hydrogen consumption; following calcination at 800°C, this value increases to 39%, and at the same time a shift of the peaks to higher temperatures can be observed, corresponding to the growth in crystal size.

The introduction of Sr ($La_{0.8}Sr_{0.2}MnO_3$ perovskite, Fig. 3B), gives rise to significant differences in the TPR profile with respect to those observed for La-Mn perovskites. This could be expected from the XRD patterns given in Fig. 1, which show a less crystalline solid, indicating that La-Sr-Mn perovskites are more difficult to form at 600°C. A higher proportion of microcrystals for La-Sr-Mn would be in agreement with the greater H_2 consumption observed at low temperatures, compared to the La-Mn sample. With a further calcination of 2 h at 800°C, a highly crystalline sample results (as demonstrated by the results of XRD analyses; see Table 1), and the low-temperature H_2 consumption during reduction decreases considerably, as can be seen in the TPR pattern shown in Fig. 3B, where the dominant feature is now the reduction peak at 710°C.

DRIFT Analysis

La-Co. Figure 4 shows the 3200–2800 cm^{-1} and 1800–1500 cm^{-1} regions of the diffuse-reflectance infrared spectrum for both single compounds and mixtures on the $LaCoO_3$ perovskite (at 210°C), together with the gas-phase curves for the individual compounds (obtained by transmission in a separate experiment). Comparing the gas-phase curve for toluene with that obtained in the presence of the $LaCoO_3$ perovskite, it can be seen that there is very little, if any, significant absorbance in the region 1650–1500 cm^{-1} (vibration of the substituted aromatic ring (15)), and only weak bands are observed in the 3100–3000 cm^{-1} (C-H stretching in aromatics), and 3000–2800 cm^{-1} (vibration of methyl group). The corresponding curves for MEK show evidence of a considerably higher amount of VOC adsorbed on the surface: The characteristic bands are clearly marked in the presence of $LaCoO_3$ and present significant shifts with respect to the positions of the corresponding gas-phase peaks. Thus, the gas-phase peak at 2992 cm^{-1} (vibration of $-CH_2-C=O$) shifts to 2980 cm^{-1} in the presence of $LaCoO_3$. In the 1800–1600 cm^{-1} region ($C=O$ stretching (14)), the main peak appears at 1709 cm^{-1}, with a shoulder at 1648 cm^{-1}. Both are displaced with respect to corresponding gas phase bands (1748 and 1723 cm^{-1}). All of this is consistent with a strong adsorption of MEK as a single compound on $LaCoO_3$.

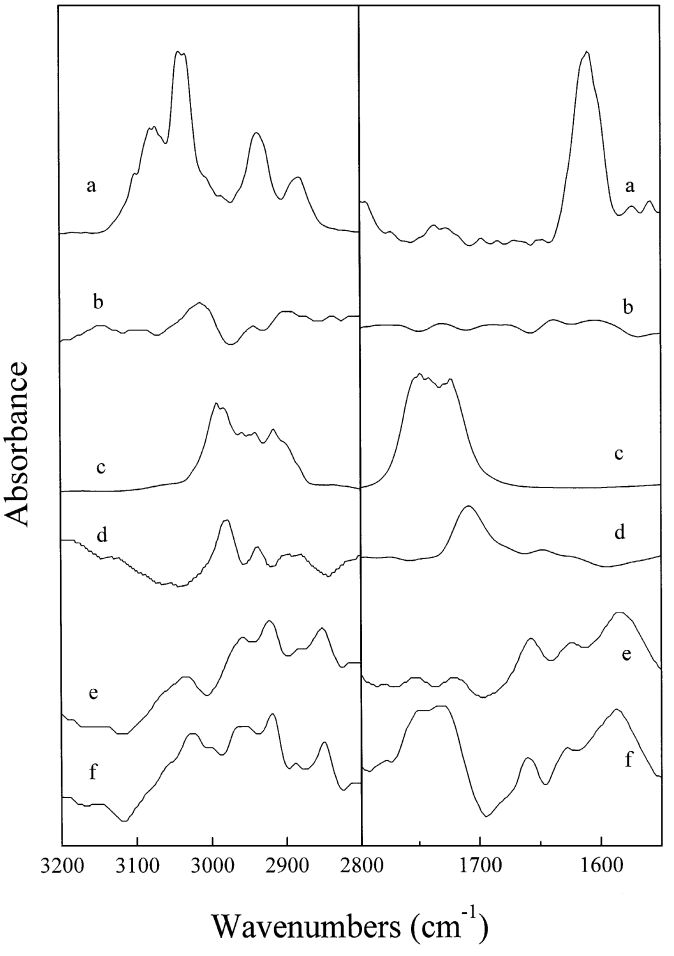

FIG. 4. Steady-state DRIFT patterns obtained on $LaCoO_3$ at 210°C. From top to bottom: **a**, toluene, gas phase; **b**, toluene, single compound; **c**, MEK, gas phase; **d**, MEK, single compound; **e**, mixture of 51% MEK and 49% toluene in air; **f**, mixture of 70% MEK and 30% toluene in air. (*Note.* The percentages in the mixture refer to the proportion of moles of carbon contributed by each organic compound and do not take into account the accompanying air.)

The simultaneous feed to toluene and MEK to the catalytic chamber significantly changes the DRIFT patterns, as shown by curves e and f in Fig. 4. It can be seen that the intensity of the bands in the 3200–2800 cm^{-1} region increase and that toluene bands in the 1650–1500 cm^{-1} region are now clearly present. The characteristic band for aromatic C-H stretching in toluene (at 3048 cm^{-1} in the gas phase) now appears well defined at 3024 cm^{-1} in the curve corresponding to the mixture with 51% concentration of MEK (51% refers to the percentage of carbon atoms corresponding to MEK in the reactor feed, while 49% were contributed by toluene). Also, the toluene gas-phase signal at 1609 cm^{-1}, which appeared only very weakly in the single-compound curve at the same frequency, is now clearly present, shifted to

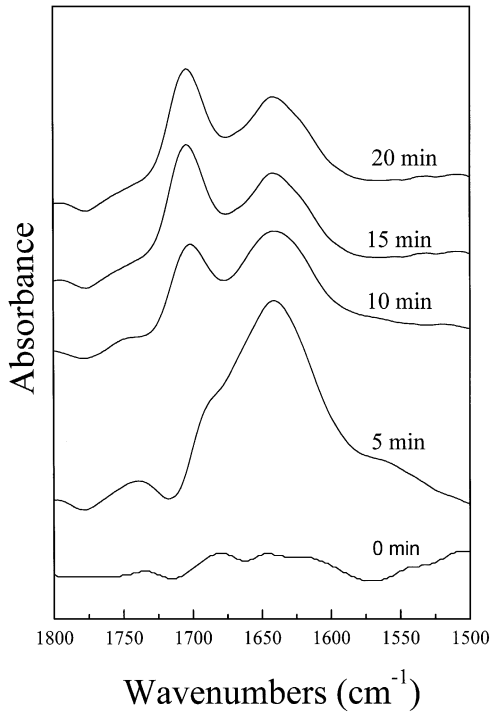

FIG. 5. Transient DRIFT patterns obtained on $LaCoO_3$ at 300°C. The sample was initially oxidized in air at the reaction temperature and then exposed to a MEK-saturated air stream (saturated at room temperature). Time zero corresponds to the introduction of the MEK-containing stream.

1586 cm^{-1}. On the other hand, the MEK peak at 2992 cm^{-1} in the gas phase, which shifted to 2980 cm^{-1} as a single compound, now shifts further, to 2966 cm^{-1}. Similar results were obtained for MEK concentrations of 63% and 70%. The increase in the intensities and the shifts in the position of the characteristic bands for toluene and MEK indicate that both compounds are now more strongly adsorbed on the catalyst surface.

In order to clarify the interaction of both VOCs with the catalyst surface, some transient DRIFT experiments were carried out in which an initially oxidized surface (oxidation in air stream at the reaction temperature) was suddenly exposed to an air stream containing either toluene or MEK, and DRIFT patterns were taken approximately every minute. The results presented in Fig. 5 are those obtained at 300°C with MEK, since as indicated above, the DRIFT bands of toluene as a single compound on $LaCoO_3$ were too weak to be used as an indication of changes on the catalyst surface. Figure 5 shows that on an oxidized surface the main peak in the 1800–1300 cm^{-1} region appears at 1641 cm^{-1}, with a shoulder around 1700 cm^{-1}. As time increases, the area of this shoulder increases to become the peak at 1709 cm^{-1} that is the dominant feature in the steady-state results (curve d of Fig. 4.2). At the same time, the intensity of the peak at 1641 cm^{-1} decreases to become almost negligible in the steady-state pattern. These results could be indicative of a reduction of the catalyst surface by gas-phase MEK at the reaction temperature. When the same experiment was run with a MEK-saturated N_2 stream instead of air (not shown), a very fast transient ensued (in fact, too fast to be followed by DRIFT at the temperatures used), leading to the steady-state peak 1709 cm^{-1}, which corresponds to the reduced surface. Fast transients were also observed with MEK-saturated air at lower temperatures, while the combination of air and a higher temperature slowed the reduction process sufficiently so that the transients could be followed.

These results suggest that MEK can adsorb on different sites (i.e., on sites prevailing on oxidized surfaces, giving adsorption bands at 1640–1650 cm^{-1}, and on sites with bands at ca 1700–1710 cm^{-1}, existing on partially reduced surfaces). The presence of MEK can change the relative proportions of these sites through its reducing effect on the catalyst surface. A similar reducing effect can be assumed for toluene, even though the reduction process of La-Co perovskites by toluene could not be followed by DRIFT for the reasons explained above. The reducing effects postulated for MEK and toluene were confirmed in separate TPR experiments, where the behavior of fresh La-Co samples was compared with that of samples exposed for 2 h at 300°C to atmospheres containing toluene or MEK, respectively (see Table 2). Figure 6 shows the results obtained over the La-Co perovskite. From the comparison of the standard sample and the sample exposed to MEK in air it was found that the H_2 consumed in the TPR experiment was approximately 28% lower for the latter (see Table 2). When the TPR experiment was carried out after exposure to MEK in N_2 the H_2 consumption was 36% lower; i.e., as could be expected, the reducing effect of MEK in an oxygen-containing atmosphere is weaker. As for toluene, it had a stronger reducing effect on the La-Co perovskite: After a 2-h treatment in a toluene-saturated air stream the decrease in H_2 consumption was 48%, which compares with 28% for a La-Co sample treated with MEK under comparable conditions. This is so despite the fact that the 2-h pretreatment was carried out with saturated streams in both cases, and therefore

TABLE 2

H_2 Consumption Calculated from the Area under the TPR Curve for Fresh Catalysts and for Catalyst Samples Treated with VOC-Saturated Air Streams

	Area under the TPR curve (a.u.)		
Perovskite	Fresh catalyst	After treatment with MEK	After treatment with toluene
La-Co	6215	4455	3200
La-Co[a]	6215	3978	
La-Sr-Co	7565	4635	3485
La-Mn	2490	1260	880
La-Sr-Mn	4000	2865	2965

[a] The MEK-saturated stream was nitrogen instead of air.

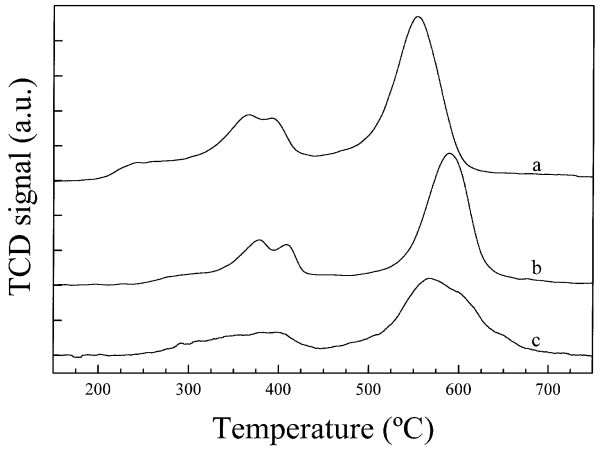

FIG. 6. Results of the temperature-programmed reduction (TPR) experiments carried out (a) with fresh $LaCoO_3$, and with $LaCoO_3$ samples exposed for 2 h at 300°C to (b) MEK-saturated and (c) toluene-saturated streams, respectively.

the gas phase concentration of MEK was considerably higher (the vapor pressure of toluene at 25°C is only about one-third that of MEK). It should be remarked that the reducing effect of both MEK and toluene was found for the four different perovskites studied in this work. Significant reductions in H_2 consumption were measured after a 2-h treatment with either of these compounds, the magnitude of the reduction ranging from 26 to 65%.

These results are useful to interpret the DRIFT patterns presented in Fig. 4. During reaction, there is an equilibrium between oxidized and reduced sites on the catalyst surface that is strongly influenced by the reaction atmosphere. In the absence of toluene and when there was a significant degree of reduction of the catalyst surface, the main peak for MEK was the "reduced site" band at 1709 cm^{-1}, while adsorption on "oxidized" sites (band at 1640–1650 cm^{-1}) was comparatively less important. However, when toluene–MEK mixtures were fed, toluene seemed to adsorb on the "reduced" sites with preference to MEK, whose adsorption on the "oxidized" sites then became more important (refer to curves e and f in Fig. 4.2).

La-Sr-Co. Figure 7 shows the DRIFT patterns obtained over the La-Sr-Co perovskite, together with the gas-phase curves for the individual species. The main difference with respect to La-Co is the stronger adsorption of toluene as a single compound, with significant adsorption in the region 1530–1560 cm^{-1} (monosubstituted aromatic ring). The intensity of this band (which was not present in the La-Co perovskite) increased in the presence of MEK, eventually decoupling into two peaks at 1542 and 1517 cm^{-1}, which reached a maximum for a MEK concentration of 70%. Otherwise, the trends observed regarding MEK adsorption were similar to those just discussed for La-Co, except for the peak at 1725 cm^{-1}, which can probably be attributed to a different adsorption mode of MEK in the presence of Sr. When toluene was present in the system (see curves for 63% and 70% MEK), MEK was again displaced from the "reduced" sites (1713 cm^{-1}), while the intensity of the band corresponding to the "oxidized" sites (1760 cm^{-1}) increased.

La-Mn and La-Sr-Mn. The trends observed were similar to those just discussed for La-Co and La-Sr-Co perovskites. The DRIFT patterns (not shown) on La-Mn indicate adsorption of both toluene and MEK as single compounds, with characteristic bands at 3059, 3031, 2929, and 2862 cm^{-1} for toluene, and 2970, 2932, 2882, 1711, and 1659 cm^{-1} for MEK, where the last two bands are characteristic of the carbonyl group for "reduced" and "oxidized" sites, respectively, the 1711 cm^{-1} band being the dominant feature for single-compound MEK. Again, when mixtures were fed, there was a considerable enhancement in the adsorption of both compounds and the intensity of the "oxidized" site band for MEK (now at 1657 cm^{-1}) increased, at the expense

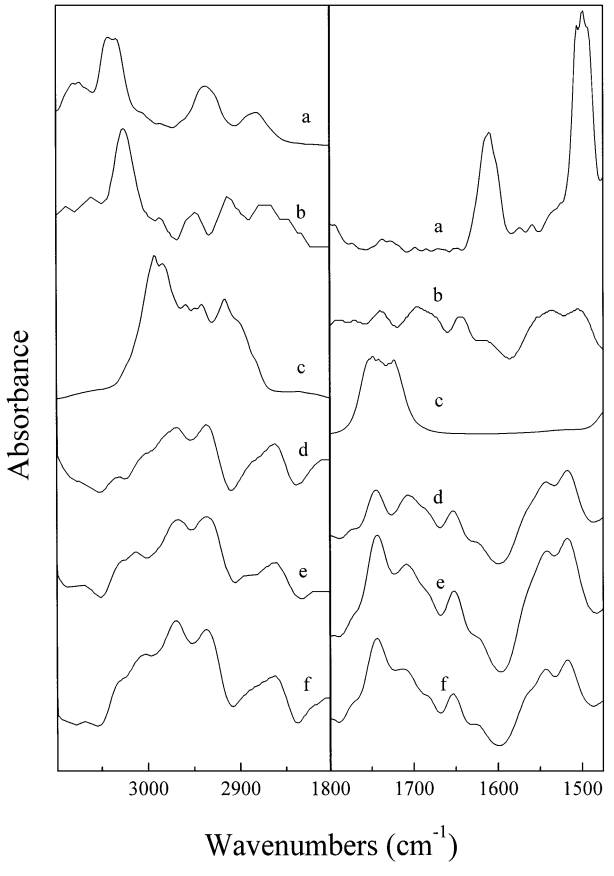

FIG. 7. Steady-state DRIFT patterns obtained on La-Sr-Co perovskite at 210°C. From top to bottom: **a**, toluene, gas phase; **b**, toluene, single compound; **c**, MEK, gas phase; **d**, MEK, single compound; **e**, mixture of 63% MEK and 37% toluene in air; **f**, mixture of 70% MEK and 30% toluene in air. (*Note.* The percentages in the mixture refer to the proportion of moles of carbon contributed by each organic compound and do not take into account the accompanying air.)

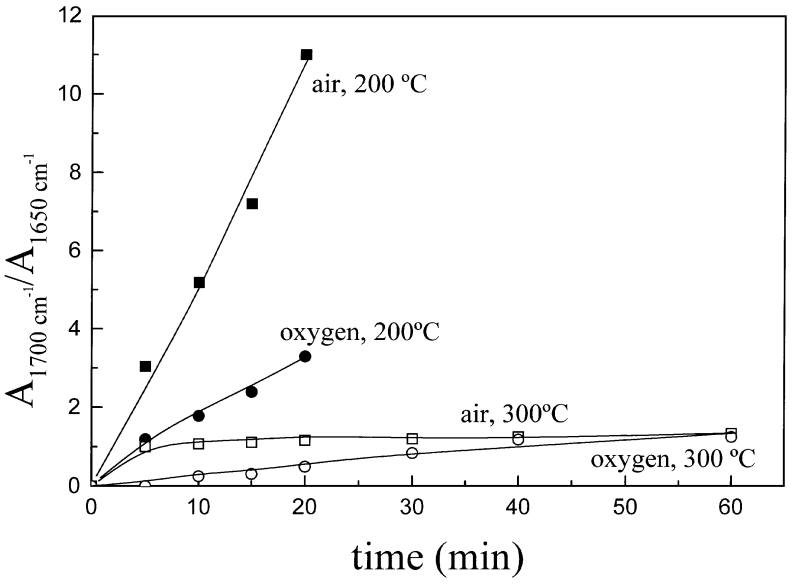

FIG. 8. Evolution of the ratio of areas of the DRIFT bands at ca 1700 and 1650 cm^{-1}, obtained by passing MEK-saturated air or oxygen streams, at two different temperatures.

of the "reduced" site band. Figure 8 shows the evolution with time of the ratio of areas of the MEK bands at ca 1700 and 1650 cm^{-1}, as obtained from DRIFT experiments carried out under different atmospheres and temperatures. As could be expected, the replacement of air by O_2 in the reaction atmosphere retards the partial reduction of the surface, as indicated by a slower increase in the ratio of peak intensities. However, the change in temperature from 200 to 300°C has a very strong effect, e.g., after 20 min, the ratio of areas of the MEK bands at 1700 and 1650 cm^{-1} under a MEK-saturated air stream is 1.2 at 300°C, which compares with a value of 11 at 200°C. This can be explained as a result of the faster oxidation of the catalytic surface at higher temperatures, which retards the process of surface reduction by MEK.

For La-Sr-Mn, DRIFT analysis (not shown), also indicated adsorption of both species as single compounds, with characteristic bands at 3060, 3028, 2925, and 2873 cm^{-1} for toluene, and 2979, 2932, 2882, 1711, and 1659 cm^{-1} for MEK. In this case the band for the "oxidized" site was not clearly visible when MEK was fed as a single compound. The trends observed for mixtures were similar to the cases previously discussed: The adsorption of toluene was enhanced, as noticed from the increased intensity of the characteristic bands and the magnitude of the shifts observed from the gas-phase values. Thus, the gas-phase bands at 1609 (aromatic ring) and 3073 and 3048 cm^{-1} (C-H stretching) now appear at 1582, 3058, and 3027 cm^{-1}. As for MEK, again the vibration band for the carbonyl group adsorbed on the "oxidized" site (at 1659 cm^{-1}) was clearly marked when the feed contained MEK/toluene mixtures instead of single-compound MEK.

Reaction Experiments

Figures 9 and 10 show respectively the conversion of toluene and MEK as a function of temperature (light-off curves) for the different perovskites studied in this work. It can be seen that the light-off (50%) and total combustion temperatures for MEK are always lower than for toluene, i.e., the reactivity of MEK on the perovskites tested is higher. A fit of the data gathered in the different kinetic experiments gives apparent reaction orders close to 0 and 1 for toluene and MEK, respectively, with relatively low apparent activation energies (39,500 to 74,000 kJ/mol) for the combustion of toluene over the different perovskites, while those for combustion of MEK were much higher (137,000 to 230,000 kJ/mol), which was to be expected in view of the higher slope of the light-off curves for MEK.

Table 3 compares the performance of the different catalysts in terms of specific reaction rate (mol/s · m^2 of BET area) for both toluene and MEK. It is interesting to

TABLE 3

Specific Reaction Rate (Moles Converted per m^2 of Surface Area per Second) for the Different Catalysts Used in This Work Measured at: $P_{VOC} = 162$ Pa, WHSV = 178 h^{-1}, $T = 255$°C for toluene; $P_{VOC} = 192$ Pa, WHSV = 186 h^{-1}, $T = 275$°C for MEK

	Specific reaction rate (moles/s ∗ m^2) ∗ 10^8			
	La-Co	La-Sr-Co	La-Mn	La-Sr-Mn
MEK	21.23	14.71	4.81	9.82
Toluene	14.92	14.12	4.88	5.67

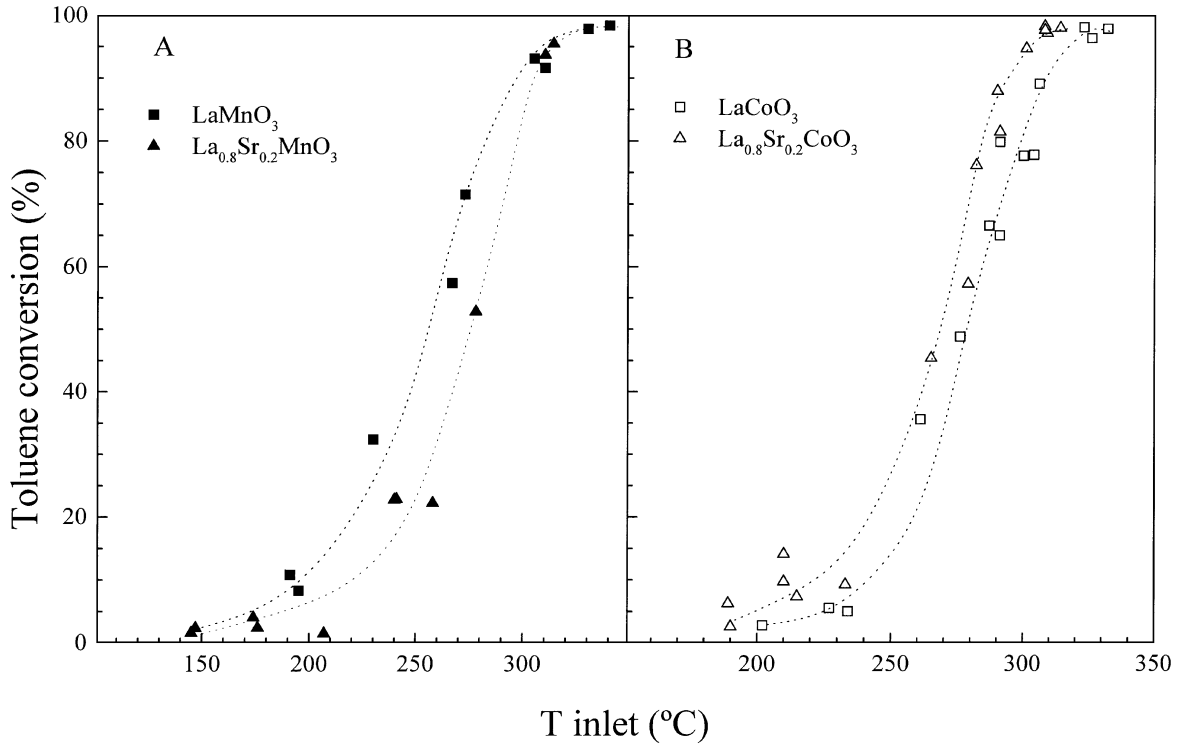

FIG. 9. Light-off curves for toluene combustion over the different perovskites studied in this work. Conditions: partial pressure of toluene 192 Pa; WHSV = 186 h^{-1}.

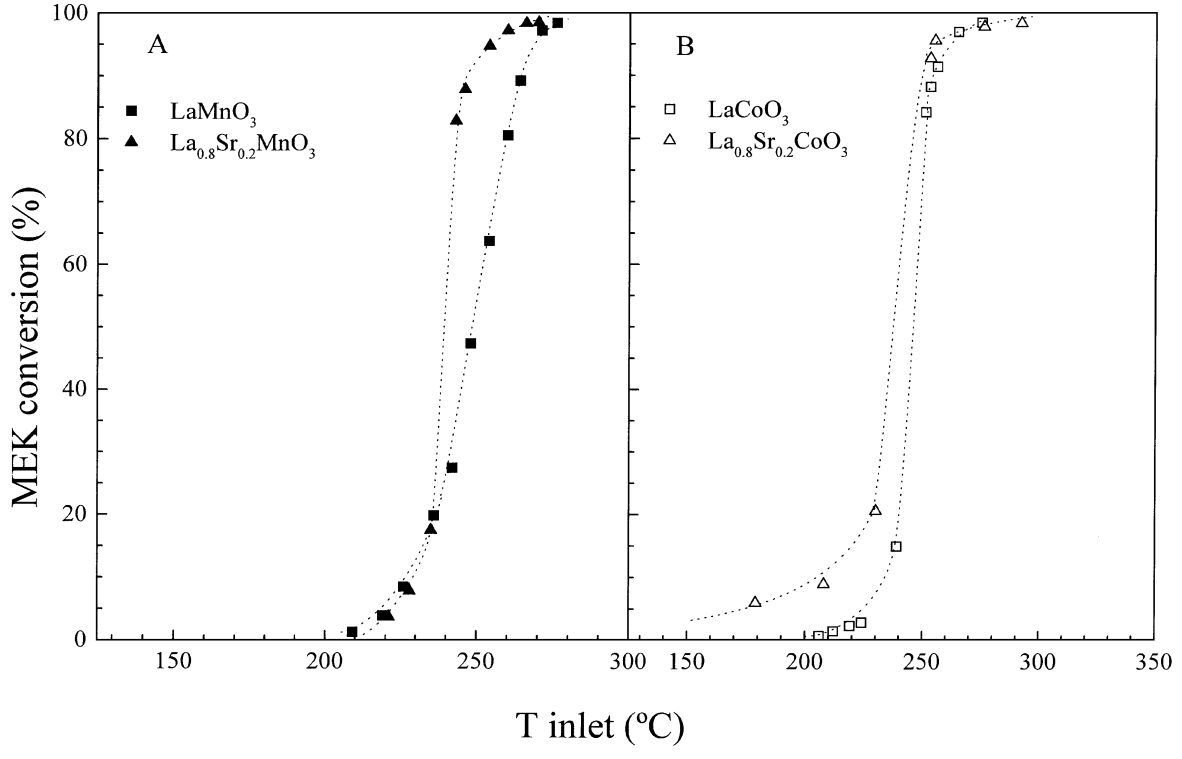

FIG. 10. Light-off curves for MEK combustion over the different perovskites studied in this work. Conditions: partial pressure of MEK 162 Pa; WHSV = 178 h^{-1}.

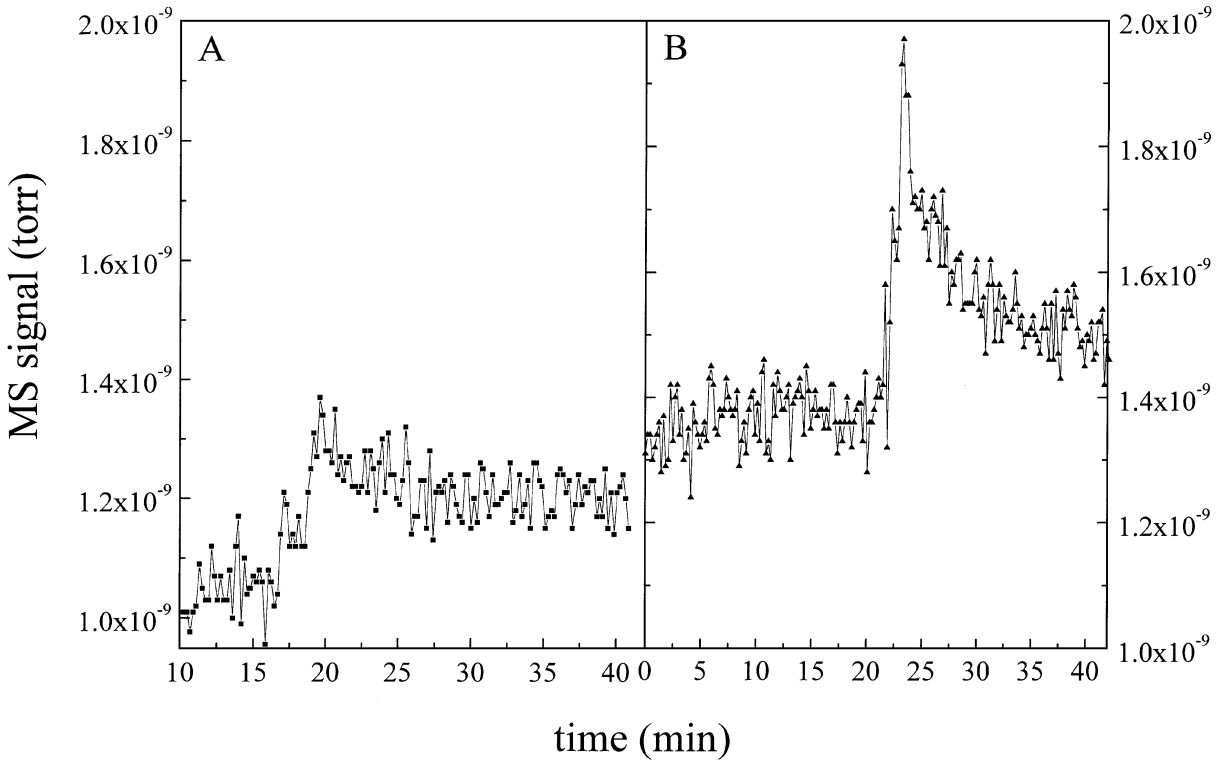

FIG. 11. Evolution of CO_2 formation during transient reaction experiments over 30 mg of La-Co perovskite at 230°C and WHSV = 185 h^{-1}. The partial pressure of MEK was 475 Pa (a) and 950 Pa (b).

observe that the addition of Sr only seems to enhance the combustion of MEK on La-Mn (the specific reaction rates are roughly doubled for the Sr-loaded perovskites), while it has no significant effect for the combustion of toluene. Also, the turnover rates were always considerably higher for La-Co than for La-Mn and for La-Sr-Co than for La-Sr-Mn; i.e., the presence of Co results in a more active combustion catalyst for both feedstocks studied, aromatics (toluene) and oxygenates (MEK).

The results presented in Figs. 9 and 10 and in Table 3 are steady-state results, i.e., obtained with a catalytic surface in equilibrium with the reaction atmosphere. Some transient reaction experiments were also run, in which an air-oxidized La-Co perovskite sample was suddenly exposed to a MEK-containing gas stream, while the exit stream from the microreactor was continuously monitored using mass spectrometry. An example of the results is shown in Fig. 11. It can be observed that, upon the introduction of MEK a transient period followed, during which the relatively high initial rate of CO_2 production decreased to reach a new stable value corresponding to a different equilibrium state on the surface. This can be related to the already discussed reduction of the La-Co perovskite by MEK. The transient period could last for up to 30 min, depending on the operating conditions.

Finally, Figs. 12 and 13 show the behavior of La-Co and La-Mn perovskites in the combustion of toluene–MEK mixtures. In both cases, the experiments were run by maintaining a constant temperature (230°C in the vicinity of the MEK light-off point) and changing the relative proportions of toluene and MEK in the mixture, while keeping an approximately constant number of carbon atoms in the feed. It can be seen that for both catalysts there was a marked increase in the total conversion as the percentage of MEK increased. Further, the conversion of MEK

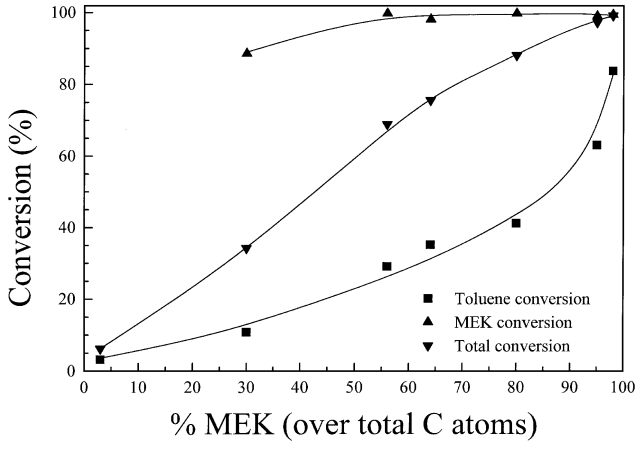

FIG. 12. Combustion of toluene–MEK mixtures at 230°C, over La-Co perovskites. Variable toluene/MEK ratio, with an approximately constant carbon-atom level in the feed, at 12,000 ppm C, WHSV = 455 h^{-1}.

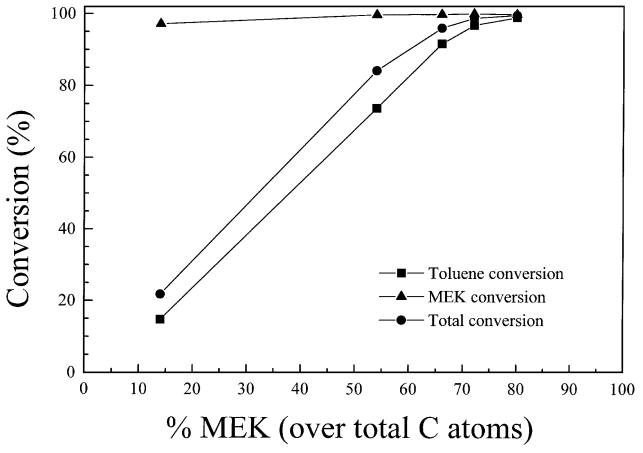

FIG. 13. Combustion of toluene–MEK mixtures at 230°C, over La-Mn perovskites. Variable toluene/MEK ratio, with an approximately constant carbon-atom level in the feed, at 18,000 ppm C, WHSV = 455 h^{-1}.

in binary MEK-toluene mixtures was considerably higher than that of MEK as a single compound: in Figs. 12 and 13 the conversion of MEK is always 90% or higher, while the corresponding values at 230°C (see the curves for La-Co and La-Mn in Fig. 10) would have been in the 5–20% range. This was confirmed in a separate experiment (not shown), which was started with a single-compound MEK. A low conversion was initially obtained, which increased as a moderate proportion of toluene was introduced in the feed. However, the most remarkable feature in Figs. 12 and 13 concerns the behavior of toluene. The light-off temperatures for toluene over La-Co and La-Mn are respectively 275 and 257°C, relatively far from the 230°C used in the experiment. In fact, at low MEK concentrations (high concentrations of toluene), the conversion of toluene is close to zero. However, as the MEK concentration was increased while maintaining a constant temperature, the toluene conversion increased rapidly, reaching high conversion values for low toluene concentrations.

Therefore, there is a positive synergistic effect (increased conversion with respect to the single-compound curves) of the simultaneous presence of toluene and MEK in the reaction atmosphere. This result has to be interpreted on the light of the changes observed on the catalyst surface when MEK-toluene mixtures were present in the reactor. DRIFT analysis showed that the simultaneous feeding of toluene and MEK markedly increased the adsorption of both compounds (especially of toluene) on the different perovskite catalysts tested. Further, the presence of toluene displaced the adsorption of MEK towards less reduced sites, which is likely the reason behind the increase in MEK conversion in the presence of toluene (Figs. 12 and 13). On the other hand, the increase in toluene conversion (and in total VOC conversion) as the MEK concentration was increased is probably the consequence of the evolution towards a less reducing atmosphere as the concentration of MEK is increased. The mass-spectrometry-monitored transient experiments demonstrated the high initial activity of an oxidized surface. Increasing the MEK concentration in the gas phase while lowering that of toluene would be expected to result in a less reduced catalyst (refer to Fig. 6 and Table 2), and therefore in a higher activity for VOC combustion. In fact, the best results with the perovskites studied in this work were obtained with mixtures of an intermediate reducing character: some reducing character is probably beneficial, in order to enhance adsorption of VOC molecules; however, a highly reducing atmosphere results in a depletion of lattice oxygen in the catalyst top layers, decreasing the combustion activity.

CONCLUSIONS

La-Co and La-Mn perovskite catalysts, with and without the addition of Sr are active for low-temperature combustion of VOCs (toluene and MEK). The method of preparation used and the addition of Sr influences the properties of the catalyst: Sr-containing perovskites are less crystalline, can be reduced at lower temperatures, and have a higher surface area. On the other hand, Co-containing perovskites were considerably more active (in terms of turnover rate) than their Mn counterparts.

The operating conditions (temperature and composition of the reacting atmosphere) have a strong effect on the state of the catalyst surface. The presence of either toluene or MEK was sufficient to partially reduce the catalyst surface. Upon the introduction of any of these compounds, significant changes could be observed on the catalyst surface which affected the balance between oxidized and (partially) reduced sites. Synergistic effects (enhancement of catalyst activity) were detected as a result of the simultaneous presence of both MEK and toluene, when introduced in suitable proportions in the reactor feed. Under these conditions the adsorption of both compounds increased, and the interaction of MEK with the catalyst surface took place mainly through oxidized, rather than reduced, sites.

ACKNOWLEDGMENTS

Financial support from DGICYT, Spain (MAT94-0499) is gratefully acknowledged. We wish to thank Drs. J. Blasco and A. Montoya for useful discussions regarding the interpretation of XRD patterns. One of the authors (S.I.) is grateful to UNL and FOMEC (Argentina) for financing her postdoctoral leave.

REFERENCES

1. Libby, W. F., *Science* **171**, 499 (1971).
2. Zwinkels, M. F. M., Järas, S. G., and Menon, P. G., *Catal. Rev. Sci. Eng.* **35**(3), 319 (1993).
3. Arai, H., Yamada, T., Eguchi, K., and Seiyama, T., *Appl. Catal.* **26**, 265 (1986).
4. Zhang, H. M., Teraoka, Y., and Yamazoe, N., *Catal. Today* **6**, 155 (1989).

5. Taguchi, H., Matsu-ura, S., Nagao, M., Choso, T., and Tasata, K., *J. Solid State Chem*. **129**, 60 (1997).
6. Barnard, K. R., Foger, K., Turney, T. W., and Williams, R. D., *J. Catal.* **125**, 265 (1990).
7. Collongue, B., Garbowski, E., and Primet, M. J., *J. Chem*. *Soc. Faraday Trans.* **87**(15), 2496 (1991).
8. Milt, V. G., Spretz, R., Ulla, M. A., Lombardo, E. A., and García Fierro, J. L., *Catal. Lett.* **42**, 57 (1996).
9. Chang, C., and Weng, H., *Ind. Eng. Chem*. *Res.* **32**, 2930 (1993).
10. Lintz, H., and Wittstock, K., *Catal. Today* **29**, 457 (1996).
11. Spivey, J., *Ind. Eng. Chem*. *Res.* **26**, 2165 (1987).
12. Barresi, A. A., and Baldi, G., *Ind. Eng. Chem*. *Res.* **33**, 2964 (1994).
13. Pina, M. P., Irusta, S., Menéndez, M., Santamaría, J., Hughes, R., and Boag, N., *Ind. Eng. Chem*. *Res.* **36**, 4557 (1997).
14. Wachowski, L., Zielinski, S., and Burewicz, A., *Acta Chim*. *Acad. Sci. Hung.* **106**(3), 217 (1981).
15. Busca, G., *Catal. Today* **27**, 457 (1996).